Amplification of Relativistic Electron Bunches by Acceleration in Laser Fields

J. Braenzel,[1,*] A. A. Andreev,[1,2] F. Abicht,[1] L. Ehrentraut,[1] K. Platonov,[3] and M. Schnürer[1,†]
[1]Max-Born-Institut, Max-Born-Str. 2a, 12489 Berlin, Germany
[2]Extreme Light Infrastructure - Attosecond Light Pulse Source (ELI-ALPS), Dugonicster 13, H-6720 Szeged, Hungary
[3]Vavilov State Optical Institute, Birzhevaya line 12, 199064 St. Petersburg, Russia
(Received 20 July 2016; published 5 January 2017)

Direct acceleration of electrons in a coherent, intense light field is revealed by a remarkable increase of the electron number in the MeV energy range. Laser irradiation of thin polymer foils with a peak intensity of $\sim 1 \times 10^{20}$ W/cm^2 releases electron bunches along the laser propagation direction that are postaccelerated in the partly transmitted laser field. They are decoupled from the laser field at high kinetic energies, when a second foil target at an appropriate distance prevents their subsequent deceleration in the declining laser field. The scheme is established with laser pulses of high temporal contrast (10^{10} peak to background ratio) and two ultrathin polymer foils at a distance of 500 μm. 2D particle in cell simulations and an analytical model confirm a significant change of the electron spectral distribution due to the double foil setup, which leads to an amplification of about 3 times of the electron number around a peak at 1 MeV electron energy. The result verifies a theoretical concept of direct electron bunch acceleration in a laser field that is scalable to extreme acceleration potential gradients. This method can be used to enhance the density and energy spread of electron bunches injected into postaccelerator stages of laser driven radiation sources.

DOI: 10.1103/PhysRevLett.118.014801

The interaction of electrons with very intense light fields as a fundamental physical phenomenon is studied with growing interest since lasers can provide extreme values of field parameters [1–5]. Here, one fundamental question is how to transform the enormous energy content and field strength of a focused powerful laser pulse into the generation of relativistic electrons. The emerging potential of the direct electron acceleration in relativistic laser fields originates from its scaling with the laser intensity. Here, the electrons undergo acceleration potential gradients of $\sim$0.1 TeV/m for $\sim$10 PW laser pulses, and it is suggested to avoid limitations by the plasma density or laser intensity [6–8] in contrast to the laser wakefield acceleration in underdense plasmas [4].

Next to the investigation of fundamental aspects of relativistic laser and electron dynamics, dense electron bunches with an ultrashort time structure and relativistic γ factors up to the order of 1000 are the basis of brilliant, coherent short wavelength light sources [4,9–12] and are suitable for ultrafast electron diffraction [13]. This prerequisite can be met if an intense and linearly polarized laser pulse interacts with a solid and leads to the emission of electron bunches within a half cycle of an optical laser field. In particular, the investigation of such laser created dense electron bunches is motivated by the search for a relativistic electron mirror upon which a second laser pulse could be reflected and then is upshifted in frequency due to the relativistic Doppler effect [11,12,14–17]. The efficiency of the relativistic backscattering process is dependent on a high density and narrow spectral distribution of the electron layer. These requirements reason recent interests in investigating laser accelerated electron bunches from solid bulk targets [2,3,18] and from ultrathin foil targets [9,19,20].

A general restriction for electron acceleration is given when electrons interact with a short light pulse without leaving its electromagnetic field, since an acceleration and deceleration is determined by the laser field envelope. Different approaches are studied to circumvent this situation: The common strategy aims for a decoupling between electrons and the light field before the deceleration in the declining laser field sets in [6], thus allowing a net gain of the kinetic energy. Such a situation is given when electrons are scattered out of a focal region due to the ponderomotive potential [21]. In order to obtain more energy from the laser field, additional concepts are exploited [2,3,9,11,18,19]. For example, the deceleration can be avoided when either the light field is reflected out of the electron trajectory [6,12,15,22] or when the electron is injected into the light field with a specific initial momentum [2,3,23,24].

In the following, we separate the laser field from the electrons before the deceleration sets in by introducing a spatial limitation for the light field. The concept was theoretically suggested [7,15]. Via intense laser-solid ultrathin foil interaction, we study the spectral distribution of the fast electrons that are accelerated in the laser propagation direction. We show that the electron number (N_e) in the high energy range is remarkably increased with the help of a second separator foil ($F2$), that was placed at some distance (L_0) behind the laser irradiated foil ($F1$). This scheme enables a postacceleration of electrons in the laser light leaking through the first foil, which later on is blocked by the second foil. Our experimental findings are analyzed

with 2D Particle In Cell (PIC) simulations, from which principle characteristics of the interaction between electrons and the laser field are derived. On the basis of this simulation we develop a theoretical model for the kinematics of an electron bunch that interacts with a transient laser pulse in a sub laser-cycle picture. In this picture, an increase of N_e in the high energy range is the consequence of limiting the duration of the interaction.

Experiments were performed with a Ti:sapphire laser at the High Field Laboratory of the Max Born Institute, delivering (30–35) fs pulses with a laser energy of 1.6 J on the target. A cross polarized wave generation front-end [25] results in a peak to amplified spontaneous emission contrast of $\leq 10^{-10}$ [high contrast (HC)] and optional by the use of a double plasma mirror, in a prepulse free contrast of $\leq 10^{-14}$ [ultrahigh contrast (UHC)]. The laser pulse was focused by an $f/2.5$ off-axis parabola to a focal FWHM size of ~ 4 μm, corresponding to a peak intensity of I_L (HC) $= 1 \times 10^{20}$ W/cm^2 (7×10^{19} W/cm^2 at UHC) and a relativistically normalized laser vector potential of $a_0 \sim 7$ ($I_L \lambda^2 = 1.37 \times 10^{18}\ {a_0}^2$ W/cm^2/μm^2), respectively, where λ is the laser wavelength. The experiments used ultrathin (12–100) nm polyvinylformal (PVF) $-(C_5H_7O_2)$ foils [26] that were adhered on stainless steel masks with holes 0.6 or 2 mm in diameter. A monolithic double-foil setup with different spacing between the foils was used [27]. Single foil experiments were enabled by prior removal of the second foil enabling a direct comparison. Fast electrons were detected in single laser pulse measurements with a magnetic spectrometer within a half angle of 1° in the laser propagation direction [28,29]. Additional measurements using image plates allowed the detection of the whole electron beam profile, divergence, and total areal dose. Details of the methods applied and additional material can be found in Ref. [27].

The electrons' spectral distribution detected from the single foil configuration exhibits a spectral maximum between (1–2) MeV, which corresponds to the approximation of the hot electron temperature: $E_T/m_e c^2 \approx (1 + a_0^2/2)^{1/2} - 1$ [32], where m_e and c are the electron mass and the speed of light, respectively. A typical spectrum is depicted in Fig. 1(a). Considering the full detection range, the integrated electron number N_e strongly depends on the applied laser contrast, while the spectral characteristics do not. In the comparison between UHC to the HC condition, a significant higher amount of electrons was detected for the HC condition [27]. At this contrast condition, weak prepulses (e.g., 10^{-7} at 50 ps) are not suppressed and the temporal pulse front starts to rise at 20 ps before pulse peak. In consequence, the target foil is preheated and starts to expand. It was shown in recent experiments for solid bulk targets and an oblique laser incidence angle that a specifically prepared plasma density gradient increases the number of emitted fast electrons [2,3] either by an injection of slow electrons into the (reflected) transient laser field and a followed acceleration, or by a resonant process in the skin layer [22,33]. This observation

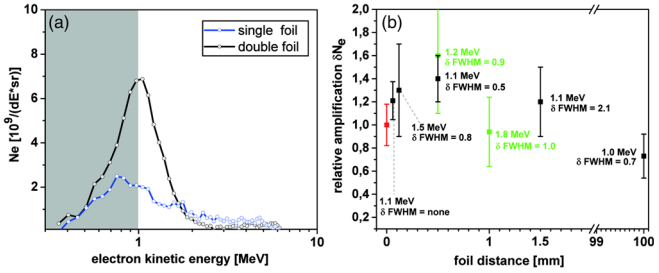

FIG. 1. (a): Detected electron spectrum from laser interaction at high temporal contrast (cf. text) with a 35 nm PVF foil and from the double foil configuration (35 nm $F1$, 90 nm $F2$) with a separation of 500 μm between the first and second foil. Gray area indicates uncalibrated energy range of detection screen. (b) Relative comparison between integrated N_e detected from double and single foil target configuration for the spectral range of 0.2 to 4 MeV and for different distances L_0 between the first and the second foil. Green refers to measurements with a target support with a hole 2 mm in diameter, black to 0.6 mm in diameter, reference to single foil configuration—red. Values at the data points give the position of the peak in the electron spectrum from single foil configuration, $\delta\text{FWHM} = \Delta E(\text{double})/\Delta E(\text{single})$ gives the ratio between the spectral bandwidth (FWHM) between double and single foil configuration. The graph summarizes different experimental runs with comparable experimental parameters except L_0.

gives an interesting insight to the concurrent laser ion acceleration, since the higher ion acceleration efficiency is obtained with the UHC condition for an optimized foil thickness [34–36].

Transmission values of the laser light of about 5%–8% were measured for the HC condition through a 90 nm PVF foil ($F1$). Hence, the transmitted light amounts to an intensity of up to $\sim 8 \times 10^{18}$ W/cm^2 behind the first foil and $> 2 \times 10^{16}$ W/cm^2 at the second foil ($F2$). This intensity level is strong enough to ionize and heat $F2$, but it is insufficient to accelerate electrons via the ponderomotive force from the second foil up to the MeV range. Following the idea of suitably separating the transmitted light field from the electron bunches, Fig. 1(a) gives a direct comparison between the electron spectra obtained from single and double foil configuration with a separation distance of $L_0 = 500$ μm and the laser at HC condition. In the presence of the second foil, a significant enhancement of N_e by a factor of 3 at the maximum of initial spectral distribution was detected. Integration over the full detection range delivered an increase of N_e of up to 1.5. Various scans (22 experimental runs with 167 single measurements) concerning different foil thickness combinations for $L_0 = 500$ μm corroborated the amplification in N_e. The integration over the full beam area with the help of IP measurements confirmed the effect [27] and excluded that a modification in the electron beam profile (e.g., focusing—a well-known effect for an electron-foil interaction [37]) leads to the observed N_e enhancement in the recorded electron spectra.

Results obtained with different separation distances are shown in Fig. 1(b) and provide further evidence that the higher amount of fast electrons is related to the copropagation of electrons in the transient laser field.

Even in a comprehensive PIC computation, the simulation box cannot account for the real dimensions of the experiment, but it can proof the feasibility of our interpretation model, and, it provides a first orientation for the development of an analytical model incorporating distance parameters of the experiment. The PIC simulation used the following laser irradiation and foil parameters:

$I_L = 10^{20}$ W cm^{-2}, $t_L = 33$ fs, a laser spot size of about $r_L = 5$ μm; the thickness of the first foil was $L1 = 45$ nm and of the second foil $L2 = 1000$ nm, with a foil distance of $L_0 = 13.5$ μm. The plasma consists of C^{6+} ions with a density of $n_i = 6 \times 10^{22}$ cm^{-3}. Computer simulations were performed with the modified code PSC [38] in 2D geometry in a 30×25 μm^2 simulation box (15000×5000 cells) with 30 particles per cell. The step size was about 2 nm in the laser propagation direction (x), 5 nm in the direction of the electric field (y), and 2 nm/c in time. The first foil was located in the simulation box at $x = 15$ μm and $F2$ at $x = 28.5$ μm.

The generation of electron bunches (2 per laser period) from the laser interaction with the first foil is shown in phase diagrams in Fig. 2(a). In this simulation, we obtained a laser transmission through the first foil of about 10%. Therefore, the released electron bunches start to copropagate with the transmitted laser pulse at an intensity of $\sim 10^{19}$ W/cm^2. The red rectangle in Fig. 2(a) selects the first 4 electron bunches 26.7 fs after the start of the simulation. In Fig. 2(b) the same bunches are marked again at later time at 37.3 fs. Comparing the maximum momentum (p_x) of these bunches at different times, one can already see a deceleration setting in for $t > 11$ fs. The second, nontransparent, foil separates the laser radiation from electrons and conserves a high electron momentum. This becomes apparent in a change in the electron spectrum and introduces a significant increase of the electron number in the energy interval between 0.5 and 3 MeV (cf., Ref. [27]). Out of this PIC simulation, the enhancement of N_e originates from a reservoir of electrons with significant lower ($\ll 0.5$ MeV) kinetic energies. Hence, the simulation showed that electrons gain energy in the radiation field between the foils, when the second foil stops the transmitted laser field and the energy exchange at a certain time. This scheme describes an electron acceleration in the copropagating laser field, which is different than the situation of an interaction with a crossed laser and electron beam at a separator foil [24]. In contrast to Ref. [24], the laser accelerates the electrons in the first instance, and the phase between electron bunches and laser light remains synchronized in the copropagation after the first foil.

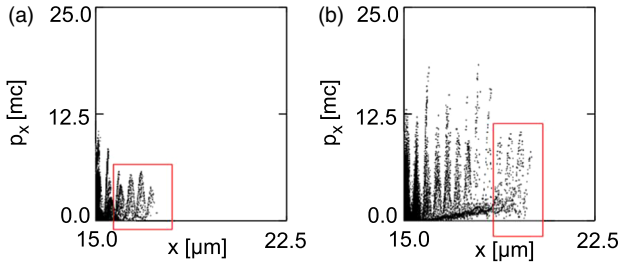

FIG. 2. Results of the PIC simulation (parameter cf. text): Phase diagram of electrons in a double foil setup with 10% transparency from the first foil, (a) at $t = 27$ fs simulation time and (b) at $t = 37$ fs simulation time. Red rectangle encloses the same group of electrons and shows their higher momentum due to interaction with the light field.

Our analytical model describes the basic acceleration scheme of an electron bunch in a transient laser field with decoupling the light field at a certain time. The number of electrons N generated from the rear side of the first foil is set as the number located in the skin layer l_s, using the condition ${\omega_{pe}}^2 l_s/2\omega c \approx a_1, N(0) \approx a_1 r_L^2 n_{cr} \lambda$, where ω_{pe} is the plasma frequency and $n_{cr} = m_e \varepsilon_0 \omega^2/q^2$ is the critical density with the elemental charge q and ε_0 as the dielectric constant in vacuum, ω the laser frequency, and a_1 corresponds to the laser intensity at the rear of the partly transparent foil of about $I_{\mathrm{LT}} = 10^{19}$ W/cm^2.

The acceleration of the electron bunch is governed by the equation of motion that permits us to find the electron bunch energy E as a function of its initial energy E_0 and position x: $E(E_0, x)$. We use the Lienard Wiechert potential to describe the electron bunch in an external vector potential $a_y^{(\mathrm{ext})}(X, \tau)$ similar to [15], where $a_y^{(\mathrm{ext})}(X, \tau)$ is the field of a linearly polarized laser pulse,

$$\frac{d}{d\theta}\left(\frac{u_y}{\sqrt{1-u_y^2-\dot{X}^2}} - a_y^{(\mathrm{ext})}(\theta)\right) = -\sigma_0 \frac{u_y}{1-\dot{X}} \frac{d}{d\theta} \frac{1-\dot{X}}{\sqrt{1-u_y^2-\dot{X}^2}} = -\sigma_0 \frac{u_y^2}{1-\dot{X}}. \quad (1)$$

Here $\tau = \omega t$, $X = \omega x/c$, the transversal velocity $u_y = v_y/c$, $\theta = \tau - X$, and $\sigma_0 = N/r_L^2 n_{cr} \lambda$ are used as normalized variables. The copropagating laser reads

$$a_y^{\mathrm{ext}}[X(\tau), \tau] = \frac{a_0 \sin(\theta)}{\sqrt{1 + X^2/(\frac{\omega L_R}{c})^2}} \exp\left(-\frac{\theta^2}{(\omega t_L)^2}\right), \quad (2)$$

where L_R is the Rayleigh length and t_L the laser pulse duration.

The normalized electron energy reads as $\gamma = \frac{1}{\sqrt{1-u_y^2-\dot{X}^2}}$, $\gamma_x = 1/\sqrt{1-\dot{X}^2}$.

First, we consider an electron layer (delta function) with an initial slow, constant kinetic energy of $E_0 = 0.2$ MeV.

The equations of motion take a finite electron bunch density $\sigma_0 = 0.05$ into account. This leads to a specific response, that is different from the single electron case, since $E(E_0, x \to \infty) \to E_0$ in the limit of $\sigma_0 \to 0$ [15]. The second foil at distance x_2 is assumed to have at least n_{cr} such that the laser light is stopped. This position corresponds to the condition, that decoupling of the electrons from the light field takes place, before the fastest electrons are overtaken by the laser pulse by more than its temporal width t_L.

Figure 3(a) shows the general dependency of the kinetic energy of the electron layer on the propagation length, calculated with Eq. (1). It is clearly visible, that at a propagation length of about 500 μm the maximum energy gain is achieved, which decreases for a longer propagation. Thus, a decoupling between electrons and the light field preserves a high kinetic energy and leads to a higher number of electrons in a distinct energy interval. Moreover, a small energy enhancement in the case of a decoupling in the fading light field is visible in Fig. 3(a) for the final value of 3000 μm. The experimental result of Fig. 1(b) reflects this behavior.

Now we consider an initial electron distribution function at the rear side of first target ($x = L1$), as in the following:

$$f(E_0, t = 0) = \frac{N(0)}{E_T} \exp(-E_0/E_T), \tag{3}$$

with E_T the hot electron temperature in the thin target foil. Here, one has to consider the spatial dispersion of the electron bunches according to their kinetic energy distribution, and on the other hand, their phase in relation to the divergent laser field which passed through the first target foil. Let us construct the solution of the kinetic equation with the initial distribution function of

$$\begin{aligned} &f(\gamma - 1, u_y, X, \tau) \\ &\quad = \int \delta(\gamma - \gamma(\mathrm{X}))\delta(u_y - u_y(\mathrm{X}))\delta(X - X(\mathrm{X})) \\ &\qquad \times f(\gamma_0, u_{y0}, X_0, 0) d\gamma_0 du_{y0} dX_0, \end{aligned} \tag{4}$$

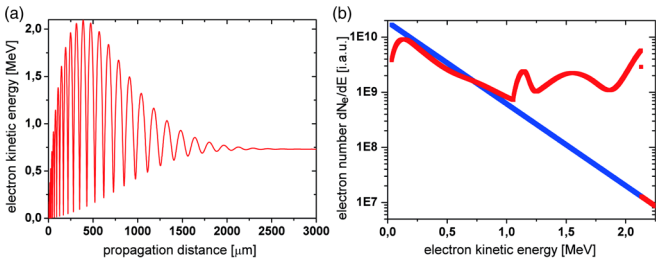

FIG. 3. (a) The energy gain of an electron bunch due to copropagation in a laser field, according to Eq. (1), with an initial low energy of 0.2 MeV and as a function of the propagation distance (parameter, cf. text). (b) The electron energy distribution function at the cutoff distance of 500 μm (red line) calculated with Eq. (5) and an initial electron spectral distribution (blue line).

where $X(\gamma_0, u_{y0}, X_0, \tau)$, $\gamma(\gamma_0, u_{y0}, X_0, \tau)$, $u_y(\gamma_0, u_{y0}, X_0, \tau)$ are the position, the energy, and the transversal velocity of the electron layer in the laser field. The initial electron energy distribution reads now $f(\gamma_0 - 1, u_{y0}, X_0, 0) = N(0) \exp[-(\gamma_0 - 1)/(E_T/mc^2)]\delta(u_{y0})\delta(X_0)$.

Finally, the electron distribution function is calculated with the "method of characteristic trajectories" [15] in respect to x_2:

$$f(E) = \frac{N(0)}{E_T} \exp\left(-\frac{E_0(E, x_2)}{E_T}\right) \left|\frac{dE_0}{dE}\right|. \tag{5}$$

The integration of Eq. (1) in X, u_y and for τ at the "cutoff" distance $x_2 = L_0\, X(\gamma_0, u_{y0}, X_0, \tau) = X_2$ is obtained, which gives the final electron energy distribution function.

Figure 3(b) shows how the electron energy distribution function changes when the second (separator) foil is placed at the distance of 500 μm, and with respect to the initial distribution of Eq. (3). Slow electrons ($E_{\mathrm{kin}} \ll 0.5$ MeV) are postaccelerated and appear in this case at higher energies.

In the experiment the electron number varies mainly in the energy interval (0.5–2) MeV when comparing between single and double foil configuration. In a qualitative agreement, the result of the model calculation [Fig. 3(b)] shows a significant and complex change in the electron spectrum between 1 and 2 MeV. In the model, the overall electron number $N_e \equiv N(0)$ does not change *per se*, because it includes the electrons in the low kinetic energy range $\ll 0.5$ MeV, which could not be accessed experimentally.

In conclusion, we presented and analyzed an experiment where a high intensity laser pulse creates electron bunches from a thin plasma sheet. A small part of the laser pulse is transmitted through the plasma and provides a postacceleration for slow electrons. We exploited the idea of a partly transparent target foil that realizes a postacceleration of electrons in vacuum with the transmitted light field. The placement of an additional second thin foil in the beam decouples the electrons from the light field and avoids a following deceleration. In consequence, a significant manipulation of the spectral distribution of the emitted relativistic electrons was observed. This scheme provides an inherent synchronization for the electron injection into the acceleration field. We showed that this process works with laser pulses with an appropriate high temporal contrast irradiating ultrathin (<200 nm) plastic foils. The setup allows increasing electron numbers in an energy range which scales with the ponderomotive energy of the laser field and produces a distinct peak in the electron energy distribution. The introduced temporal limitation of the copropagation between electrons and the light field enabled an energy transfer to the electrons, such that it appears as an amplification of the electron number in a narrow energy interval. With the developed theoretical model, it is possible to extrapolate the scheme to laser intensities accessible with the next generation of ultraintense laser systems. Intensities

of the order of 10^{22} W/cm^2 are predicted to produce dense electron bunches at GeV kinetic energy, which could be enhanced several times in number and energy due to a light field enclosed in a double foil setup. This parameter range holds the potential for the generation of extremely bright bursts of ultrashort x-ray flashes since the efficiency of relativistic backscattering schemes demands quasimonoenergetic dense electron bunches.

The research leading to these results received funding from the Deutsche Forschungsgemeinschaft within the program CRC/Transregio 18 and LASERLAB-EUROPE (Grant No. 284464, EC's Seventh Framework Program). Computational resources were provided by the ISC within Project No. MBU15 and by the John von Neumann Institute for Computing (NIC) providing us access on JUROPA at the Jülich Supercomputing Centre (JSC). Furthermore we thank D. Sommer (MBI) for his excellent work on the target production and A. Pittlik (DGZfP—Berlin, Adlershof) for providing an image plate scanner.

*braenzel@mbi-berlin.de
†schnuerer@mbi-berlin.de

[1] A. Di Piazza, C. Müller, K. Z. Hatsagortsyan, and C. H. Keitel, Rev. Mod. Phys. **84**, 1177 (2012).
[2] M. Bocoum, M. Thévenet, F. Böhle, B. Beaurepaire, A. Vernier, A. Jullien, J. Faure, and R. Lopez-Martens, Phys. Rev. Lett. **116**, 185001 (2016).
[3] M. Thevenet, A. Leblanc, S. Kahaly, H. Vincenti, A. Vernier, F. Quere, and J. Faure, Nat. Phys. **12**, 355 (2016).
[4] W. P. Leemans *et al.*, Phys. Rev. Lett. **113**, 245002 (2014).
[5] T. Tajima and J. M. Dawson, Phys. Rev. Lett. **43**, 267 (1979).
[6] K. P. Singh, Phys. Plasmas **11**, 3992 (2004).
[7] P. X. Wang, Y. K. Ho, X. Q. Yuan, Q. Kong, N. Cao, A. M. Sessler, E. Esarey, and Y. Nishida, Appl. Phys. Lett. **78**, 2253 (2001).
[8] Y. I. Salamin and C. H. Keitel, J. Phys. B **33**, 5057 (2000).
[9] D. Kiefer *et al.*, Nat. Commun. **4**, 1763 (2013).
[10] F. V. Hartemann, D. J. Gibson, W. J. Brown, A. Rousse, K. T. Phuoc, V. Mallka, J. Faure, and A. Pukhov, Phys. Rev. ST Accel. Beams **10**, 011301 (2007).
[11] T. Zh. Esirkepov, S. V. Bulanov, M. Kando, A. S. Pirozhkov, and A. G. Zhidkov, Phys. Rev. Lett. **103**, 025002 (2009).
[12] H. C. Wu, J. Meyer-ter-Vehn, J. Fernández, and B. M. Hegelich, Phys. Rev. Lett. **104**, 234801 (2010).
[13] A. J. Goers, G. A. Hine, L. Feder, B. Miao, F. Salehi, J. K. Wahlstrand, and H. M. Milchberg, Phys. Rev. Lett. **115**, 194802 (2015).
[14] S. S. Bulanov, A. Maksimchuk, K. Krushelnick, K. I. Popov, V. Y. Bychenkov, and W. Rozmus, Phys. Lett. A **374**, 476 (2010).
[15] A. A. Andreev, P. K. Yu, and K. Platonov, Quantum Electron. **43**, 435 (2013).
[16] W. J. Ma *et al.*, Phys. Rev. Lett. **113**, 235002 (2014).
[17] S. V. Bulanov, T. Z. Esirkepov, M. Kando, and J. Koga, Plasma Sources Sci. Technol. **25**, 053001 (2016).
[18] L. Fedeli *et al.*, Phys. Rev. Lett. **116**, 015001 (2016).
[19] D. Kiefer *et al.*, Eur. Phys. J. D **55**, 427 (2009).
[20] A. Henig *et al.*, Phys. Rev. Lett. **103**, 245003 (2009).
[21] F. V. Hartemann, S. N. Fochs, G. P. Le Sage, N. C. Luhmann, J. G. Woodworth, M. D. Perry, Y. J. Chen, and A. K. Kerman, Phys. Rev. E **51**, 4833 (1995).
[22] P. Mulser, D. Bauer, and H. Ruhl, Phys. Rev. Lett. **101**, 225002 (2008).
[23] I. Y. Dodin and N. J. Fisch, Phys. Rev. E **68**, 056402 (2003).
[24] T. Plettner, R. L. Byer, E. Colby, B. Cowan, C. M. S. Sears, J. E. Spencer, and R. H. Siemann, Phys. Rev. Lett. **95**, 134801 (2005).
[25] M. Kalashnikov, K. Osvay, R. Volkov, H. Schönnagel, and W. Sandner, *CLEO:2011—Laser Applications to Photonic Applications* (Optical Society of America, Baltimore, MD, 2011), paper CWG3.
[26] J. Braenzel, C. Pratsch, P. Hilz, C. Kreuzer, M. Schnurer, H. Stiel, and W. Sandner, Rev. Sci. Instrum. **84**, 056109 (2013).
[27] See Supplemental Material at http://link.aps.org/supplemental/10.1103/PhysRevLett.118.014801 for measurement methods, profiles of electron emission and simulation add-on, which includes Refs. [28–31].
[28] A. Buck *et al.*, Rev. Sci. Instrum. **81**, 033301 (2010).
[29] K. Nakamura, A. J. Gonsalves, C. Lin, A. Smith, D. Rodgers, R. Donahue, W. Byrne, and W. P. Leemans, Phys. Rev. ST Accel. Beams **14**, 062801 (2011).
[30] H. Chen *et al.*, Rev. Sci. Instrum. **79**, 033301 (2008).
[31] K. Zeil, S. D. Kraft, A. Jochmann, F. Kroll, W. Jahr, U. Schramm, L. Karsch, J. Pawelke, B. Hidding, and G. Pretzler, Rev. Sci. Instrum. **81**, 013307 (2010).
[32] T. Kluge, T. Cowan, A. Debus, U. Schramm, K. Zeil, and M. Bussmann, Phys. Rev. Lett. **107**, 205003 (2011).
[33] T. Liseykina, P. Mulser, and M. Murakami, Phys. Plasmas **22**, 033302 (2015).
[34] A. Macchi, S. Veghini, and F. Pegoraro, Phys. Rev. Lett. **103**, 085003 (2009).
[35] S. Steinke *et al.*, Phys. Rev. ST Accel. Beams **16**, 011303 (2013).
[36] T. Esirkepov, M. Yamagiwa, and T. Tajima, Phys. Rev. Lett. **96**, 105001 (2006).
[37] G. Hairapetian, P. Davis, C. E. Clayton, C. Joshi, S. C. Hartman, C. Pellegrini, and T. Katsouleas, Phys. Rev. Lett. **72**, 2403 (1994).
[38] A. J. Kemp and H. Ruhl, Phys. Plasmas **12**, 033105 (2005).